RESEARCH ARTICLE

CrossMark
click for updates

Mitochondrial Heat Shock Protein Machinery Hsp70/Hsp40 Is Indispensable for Proper Mitochondrial DNA Maintenance and Replication

Jiří Týč,[a] Michele M. Klingbeil,[b] Julius Lukeš[a,c]

Faculty of Sciences, University of South Bohemia and Biology Centre, Institute of Parasitology, Czech Academy of Sciences, České Budějovice (Budweis), Czech Republic[a]; Department of Microbiology, Morrill Science Center, University of Massachusetts, Amherst, Massachusetts, USA[b]; Canadian Institute for Advanced Research, Toronto, Ontario, Canada[c]

ABSTRACT Mitochondrial chaperones have multiple functions that are essential for proper functioning of mitochondria. In the human-pathogenic protist *Trypanosoma brucei*, we demonstrate a novel function of the highly conserved machinery composed of mitochondrial heat shock proteins 70 and 40 (mtHsp70/mtHsp40) and the ATP exchange factor Mge1. The mitochondrial DNA of *T. brucei*, also known as kinetoplast DNA (kDNA), is represented by a single catenated network composed of thousands of minicircles and dozens of maxicircles packed into an electron-dense kDNA disk. The chaperones mtHsp70 and mtHsp40 and their cofactor Mge1 are uniformly distributed throughout the single mitochondrial network and are all essential for the parasite. Following RNA interference (RNAi)-mediated depletion of each of these proteins, the kDNA network shrinks and eventually disappears. Ultrastructural analysis of cells depleted for mtHsp70 or mtHsp40 revealed that the otherwise compact kDNA network becomes severely compromised, a consequence of decreased maxicircle and minicircle copy numbers. Moreover, we show that the replication of minicircles is impaired, although the lack of these proteins has a bigger impact on the less abundant maxicircles. We provide additional evidence that these chaperones are indispensable for the maintenance and replication of kDNA, in addition to their already known functions in Fe-S cluster synthesis and protein import.

IMPORTANCE Impairment or loss of mitochondrial DNA is associated with mitochondrial dysfunction and a wide range of neural, muscular, and other diseases. We present the first evidence showing that the entire mtHsp70/mtHsp40 machinery plays an important role in mitochondrial DNA replication and maintenance, a function likely retained from prokaryotes. These abundant, ubiquitous, and multifunctional chaperones share phenotypes with enzymes engaged in the initial stages of replication of the mitochondrial DNA in *T. brucei*.

Address correspondence to Julius Lukeš, jula@paru.cas.cz.

This article is a direct contribution from a Fellow of the American Academy of Microbiology.

The mitochondrion is a center of numerous essential metabolic processes of a typical eukaryotic cell. From the genomic content of its proteobacterial predecessor, the mitochondrion retained only a few genes, such as those coding for subunits of respiratory chain complexes and ribosomal proteins, while majority of its original coding capacity was transferred to the nucleus. In humans, impairment or loss of mitochondrial (mt) DNA (mtDNA) is associated with mt dysfunction and a wide range of neural, muscular, and other diseases (1–5). Therefore, understanding the maintenance and replication of mtDNA is of fundamental importance.

Mitochondrial Hsp70 (mtHsp70) and mtHsp40 are organellar versions of heat shock proteins 70 and 40. Interestingly, mtHsp70 is more closely related to the DnaK bacterial homologue than to its eukaryotic cytosolic counterparts (6). A typical mitochondrion contains a single type of Hsp70 (7), which takes part in several essential processes, such as folding of newly synthesized as well as damaged and aggregated proteins and degradation of denatured and unstable proteins (8, 9). Moreover, mtHsp70 gained new functions, such as participation in Fe-S cluster biogenesis (10, 11) and protein import across the organellar double membrane (12, 13). In some eukaryotes, such as in *Trypanosoma brucei*, additional specialized functions are associated with mtHsp70, including its participation in the importation of tRNA into the mitochondrion (14). This is a consequence of the lack of tRNA genes in the mtDNA of this and related flagellates, which thus have to be imported from the cytosol (15).

For its multiple functions, Hsp70 makes use of its ATPase domain to hydrolyze ATP. As a consequence, the Hsp70 protein oscillates between the ATP-bound state, with low affinity for hydrophobic peptides, and the ADP-bound state, with high affinity for these substrates (16). MtHsp70 does not act alone, as cochaperones and other partners are required for its proper functioning. Prominent among them is Mge1 (mt GrpE) (Table 1), a nucleo-

TABLE 1 Overview of gene nomenclature

Gene	Organism(s)	Specific designation	Function
mtHsp70	*Escherichia coli*	DnaK	General
	Saccharomyces cerevisiae	Ssc1	General
	Saccharomyces cerevisiae	Ssq1	Fe-S cluster synthesis
	Saccharomyces cerevisiae	Ecm10	Unknown
mtHsp40	*Escherichia coli*	DnaJ	General
	Saccharomyces cerevisiae	Mdj1	General
	Mammals	Tid1	General
Mge1	*Escherichia coli*	GrpE	General
	Saccharomyces cerevisiae	Mge1	General
	Homo sapiens	GRPEL1	General

tide exchange factor indispensable for all processes in which mtHsp70 is involved (17–19). Its primary function is to release ADP from mtHsp70, thus ensuring its conformational cycling. The J proteins constitute another group of interacting partners of mtHsp70 with specialized tasks. These homologues of the bacterial DnaJ protein contain so-called J and Zn-finger domains, which provide the specificity of each reaction (20). For example, in the yeast *Saccharomyces cerevisiae*, mtHsp40 (Mdj1; Table 1) is involved in protein folding (8), and Jac1 is essential for Fe-S cluster biogenesis (11), whereas the truncated Pam16 and Pam18, containing only the J domain, act in protein transport (21).

There are three copies of mtHsp70 in the *T. brucei* genome which are 100% identical on the amino acid level (22). In comparison, the *S. cerevisiae* genome also contains three paralogs of Hsp70, labeled Ssc1, Ssq1, and Ecm10, which differ in both sequence and function (Table 1) (8). It seems that in *S. cerevisiae*, Ssc1 took over most functions associated with mtHsp70, while Ssq1 specializes in functions related to Fe-S cluster biogenesis (23). Finally, the exact function of Ecm10, which localizes into the mt nucleoids and whose overexpression induces aggregation of mtDNA (24), remains to be determined, but it seems to overlap that of Ssc1 (25).

The association with mtDNA is one of the least understood properties of mtHsp70. The conjecture that the mtHsp70/mtHsp40 machinery has an important role in mtDNA replication and maintenance comes from studies of both the prokaryotic and mitochondrial systems. The prokaryotic paralog of mtHsp70, DnaK, acts in the replication of *Escherichia coli* chromosomal DNA (26), and machinery composed of DnaK, DnaJ, and GrpE was shown to be involved in both plasmid DNA replication (27) and bacteriophage DNA replication (28). Moreover, all three *E. coli* DnaJ paralogs of the mtHsp40 proteins are able to bind DNA (29).

In eukaryotes, several lines of evidence suggest that there is a physical and functional connection between mtDNA and the mtHsp70 machinery. MtHsp70 was identified as part of the mtDNA nucleoid in the yeast *Kluyveromyces lactis* (30) and in human cells (31, 32), while it is the Ecm10 paralog (24) and a portion of Ssc1 that localize to the mt nucleoid in *S. cerevisiae* (33). In kinetoplastid flagellates *Trypanosoma cruzi* (34) and *Crithidia fasciculata*, mtHsp70 colocalizes with the condensed mtDNA network (35). Following a heat shock in *S. cerevisiae*, the mtHsp70/mtHsp40 machinery was shown to facilitate the protection of organellar DNA via stabilizing the activities of mtDNA maintenance proteins, such as the mtDNA polymerase (36, 37). The deletion of Mdj1 transforms yeast cells even under normal physiological conditions into petite mutants with nonfunctional (*rho*-negative [*rho⁻*]) mtDNA (36). Similar results were reported for the mammalian Tid1 protein (Table 1), which also localizes to mt nucleoids in human cells (38). Its deficiency in mice leads to the reduction of mtDNA, causing cardiomyopathy (39). Recently, Mdj1 was shown to directly bind mtDNA in yeast and to possibly act to recruit Ssc1 to the mt nucleoid (33).

T. brucei, the causative agent of a lethal human sleeping sickness in Africa (40), is a suitable model for studying the relationship between mtHsp70 and mtHsp40 on one side and mtDNA on the other, as this early-branching protist bears a single large mitochondrion per cell and its extensive mtDNA network is concentrated into a single, ultrastructurally prominent structure called kinetoplast DNA (kDNA). Unlike most eukaryotes, which replicate their mtDNA throughout the cell cycle, kDNA replicates and segregates into daughter networks during a defined time frame prior to nuclear division (41, 42).

The kDNA is an intricate structure composed of two types of circular DNA molecules: maxicircles, which exist in dozens of identical copies and carry protein-coding genes and 9S and 12S mitoribosomal RNAs, and minicircles, which differ in sequence and are present in thousands of copies (43). Minicircles encode an extremely wide variety of guide (g) RNA genes, which provide information for the multiple insertions and/or deletions of uridines in mt transcripts via the process of RNA editing (44, 45). In *T. brucei* and related trypanosomatid flagellates, maxicircles and minicircles are interlocked into a single highly compact DNA network and attached via the tripartite attachment complex to the basal body of the single flagellum (46). The structure and replication of kDNA have been well studied, and extensive protein machinery related to these processes has been described (43).

In this study, we show that the mtHsp70/mtHsp40 machinery in *T. brucei* is an important component of the kDNA replication and maintenance apparatus, with cells lacking these chaperones being unable to faithfully propagate their kDNA. The mtHsp70, mtHsp40, and Mge1 proteins colocalize throughout the mt lumen, and their RNA interference (RNAi)-mediated depletion has a massive impact on both kDNA maxicircles and kDNA minicircles. Moreover, we provide evidence that this indispensable role of the mtHsp70/mtHsp40 machinery is independent of other functions of mtHsp70 in Fe-S cluster synthesis and protein import described so far.

RESULTS

mtHsp70/mtHsp40 machinery. The *T. brucei* mitochondrion contains three copies of mtHsp70 in its nuclear genome (7, 22, 47). However, since their predicted amino acid sequences are identical, the situation is reminiscent of most other eukaryotes which harbor a single mtHsp70 (7). These genes are products of duplication, as they are all situated in a single tandem array (*T. brucei* 927.6.3740 [Tb927.6.3740], Tb927.6.3750, and Tb927.6.3800) (48). On the basis of an *in silico* prediction, they have somewhat different 5′ and 3′ untranslated regions (data not shown); however, there is no experimental evidence on whether these differences are functional. The amplification of the mtHsp70 genes is apparently a rather frequent event in kinetoplastids with a full genome sequence available, in which the copy number ranges from 2 to 6 depending on the species (48–50).

The other two proteins of the machinery, mtHsp40 and Mge1, were identified using *S. cerevisiae* and human mtHsp40 and Mge1 protein sequences as queries for a search of the *T. brucei* genome. Using both simple BLAST and HMMER searches, genes Tb927.9.12730 and Tb927.6.2170 have been identified, respectively. According to the Mitoprot and TargetP programs, their N termini are predicted to carry an mt import signal, and the respective proteins were indeed found in the mitoproteome of *T. brucei* (51).

MtHsp70/mtHsp40 machinery is important for cell viability. Functional analysis of all three proteins (mtHsp70, mtHsp40, and Mge1) was initiated using RNAi-mediated depletion, which revealed that they are all essential for the growth of the procyclic stage of *T. brucei* (Fig. 1). This life cycle stage is particularly suitable for functional analysis of mt proteins with a conserved function, as its organelle has activity and function comparable with those of most other single-cell and multicellular eukaryotes (52). As often reported in *T. brucei*, some cells eventually become resistant to RNAi, resulting in a recovery phenotype, as was the case for mtHsp70 RNAi a few days after induction (Fig. 1A and B). A comparison of two mtHsp70 RNAi cell lines, generated using different RNAi vectors (see Materials and Methods), showed a significant growth difference after RNAi induction. The first cell line had moderate growth and recovery phenotypes starting on days 2 and 4 after RNAi induction, respectively (Fig. 1B). The second cell line produced a more severe growth phenotype which had already commenced on day 1, with the recovery phenotype emerging on day 6 after RNAi induction (Fig. 1A) (14). The ablation of Mge1 resulted in a strong growth defect that became apparent 2 days after RNAi induction and from which the cells did not recover (Fig. 1E). Depletion of mtHsp70 or Mge1 caused division arrest quite early (Fig. 1A, B, and E) and was possibly due to several processes being affected. In contrast, ablation of the mtHsp40 protein (either wild type or protein C epitope-tobacco etch virus-protein A epitope [PTP] tagged) showed a milder growth arrest (Fig. 1C and D), comparable to that seen with depletion of known kDNA replication proteins (53–57).

The efficiency of RNAi-mediated downregulation of all studied proteins was determined by Western blot analysis (Fig. 1B, D, and E). Using specific antibodies against the *T. brucei* mtHsp70 protein, we showed that the target was significantly depleted on day 2, became undetectable on day 4, and reappeared following day 6 after RNAi induction (Fig. 1B). The same approach was used to follow the level of Mge1, which was already undetectable on day
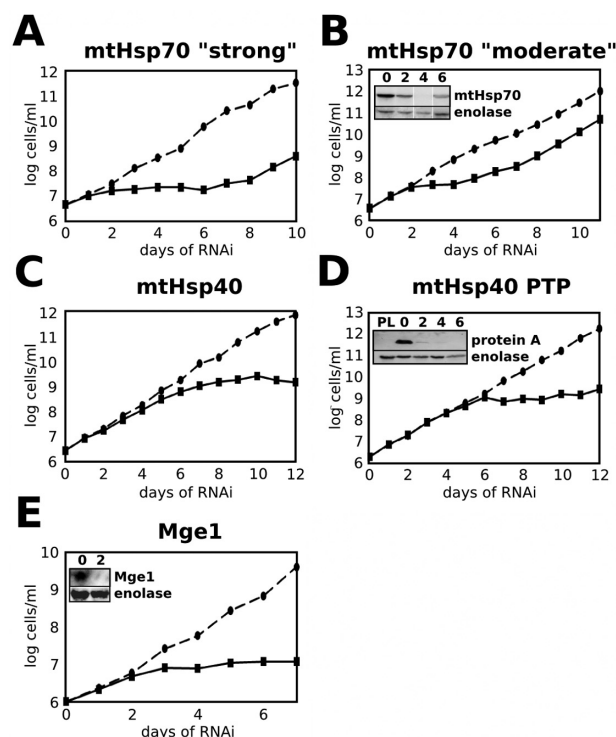

FIG 1 Components of mtHsp70/mtHsp40 machinery are essential for growth of procyclic *T. brucei*. Growth curves of cell lines induced for RNAi were calculated. (A and B) Two cell lines, in which mtHsp70 is targeted by different RNAi vectors, differ in the strength of obtained phenotype (data presented in panel A were previously described in reference 14). (C) RNAi cell line for mtHsp40. (D) RNAi cell lines for mtHsp40, in which one mtHsp40 allele was replaced by PTP-tagged mtHsp40. (E) RNAi cell line for Mge1. Uninduced cells are visualized by circles and a dashed line; cells in which RNAi against the respective genes was induced are shown by squares with a full line. (Insets) Western blot showing downregulation of the target protein, with enolase used as a loading control. Days after RNAi induction are also indicated. "PL" stands for that parental RNAi cell line, which does not express the PTP-tagged protein.

2 of RNAi induction (Fig. 1E). In the absence of a specific antibody, the depletion of mtHsp40 was checked in a cell line engineered to endogenously express the PTP-tagged mtHsp40 protein from a single allele. The tagged cell line behaved the same as the parental knockdown cells (Fig. 1C), with the tagged protein being efficiently depleted (Fig. 1D). In these cells, PTP-tagged mtHsp40 was hardly detectable on day 2 and was undetectable by the 6th day of RNAi (Fig. 1D).

Localization of mtHsp70/mtHsp40 machinery. Subcellular localization of the studied proteins was assayed by immunofluorescence using monoclonal anti-mtHsp70 antibody (58) as well as anti-protein A antibody, which allowed visualization of the PTP-tagged versions of mtHsp70, mtHsp40, and Mge1. In all cases, the whole reticulated mitochondrion was stained, showing colocalization with the mt marker Mitotracker Red (Fig. 2). The DAPI (4′,6-diamidino-2-phenylindole) staining, which prominently labels kDNA, further confirmed the identity of the organelle (Fig. 2). Next, we wondered whether localization of these proteins was subject to changes in response to the cell cycle of procyclic *T. brucei*, as recently described for another kDNA replication protein (59). However, using immunofluorescence microscopy, no major alterations were observed (data not shown).
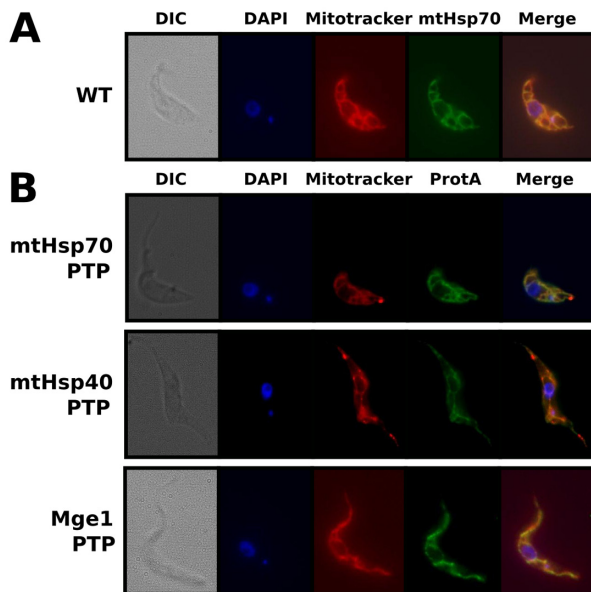
FIG 2 MtHsp70, mtHsp40, and Mge1 are present within the whole mitochondrial tubular network and colocalize with Mitotracker Red. (A) The mtHsp70 endogenous protein was visualized by using a specific monoclonal antibody. (B) In the other cell lines, the target protein was allelically tagged using PTP and subsequently detected using anti-protein A antibody (ProtA). DIC, differential interference contrast.

FIG 3 Cells depleted for mtHsp70/mtHsp40 machinery lose kDNA. (A and B) Two cell lines, in which mtHsp70 is targeted by different RNAi vectors, differ in the strength of obtained phenotype. (C and D) Two cell lines in which either wild-type or PTP-tagged mtHsp40 is targeted by RNAi. (E) Cell line with Mge1 depleted by RNAi. Circles and a solid line show cells with a normally sized kDNA, triangles and a dashed line represent cells with a small kDNA, and squares with a dotted line depict cells without kDNA (i.e., akinetoplastic cells). Cells were fixed on the slides stained by DAPI and observed under a light microscope. A minimum of 300 cells were counted per time point, and multiple focal planes were checked. (F) Uninduced cells with wild-type kinetoplast (k) with signal even stronger than the nuclear one (N). (G) A representative picture of RNAi-induced cells with significantly smaller kDNA (sk). The two images in panels F and G are equally overexposed in order to visualize the signal of small kDNA. Scale bar, 5 μm.

Depletion of mtHsp70 or mtHsp40 leads to kDNA loss. Since there is a physical connection between mtHsp40 and the mtDNA in yeast and mammals, we wondered whether ablation of this protein might cause any defects in the structure of kDNA. For that purpose, both fluorescence and transmission electron microscopy (TEM) were used. Indeed, after depletion of mtHsp70, mtHsp40, or Mge1, cells lost their kDNA, as revealed by DAPI staining (Fig. 3). Per time point of the RNAi induction, at least 300 individual cells were counted under a fluorescence microscope and divided into three categories: (i) those with normal kDNA (standard-size kDNA networks, with the DAPI signal stronger than the nuclear one); (ii) those with small kDNA (networks with at least half-size kDNA, the signal of which was weaker than that of the nucleus); and (iii) cells totally lacking kDNA (no DAPI signal other than the nuclear one could be observed). Multiple focal planes were checked, and differential interference contrast was used to confirm the cellular integrity of all analyzed cells. Examples of standard kDNA and small kDNA are shown in Fig. 3F and G, respectively.

The phenotype observed in the "moderate" mtHsp70 cell line commenced on day 2 after RNAi induction, featuring 62% flagellates with small kDNA. On the following day, the proportion of cells containing diminished kDNA grew to 75%, and, on day 4, up to 16% of trypanosomes lost the kDNA altogether (Fig. 3B). The phenotype observed in the "severe" mtHsp70 RNAi cell line was comparable, with 10% of cells already carrying small kDNA on day 1 after RNAi was triggered. Within the following 24 h, the proportion of cells containing small kDNA grew to 65%, and 5% of cells lacked kDNA altogether, becoming so-called akinetoplastic flagellates. On days 4 and 6 after RNAi induction, the culture stabilized at 50% and 30% of cells with small and no kDNA, respectively (Fig. 3A). In trypanosomes exhibiting RNAi depletion
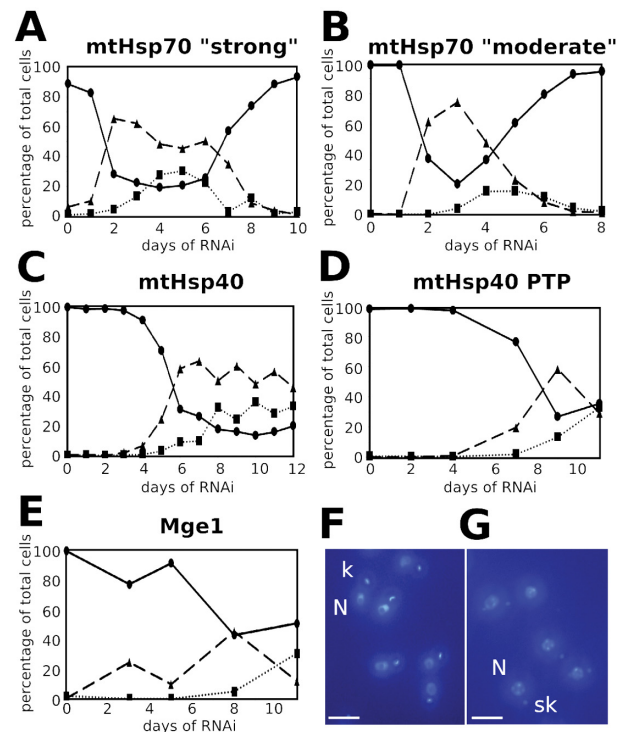
for mtHsp40, the reduction of kDNA started on day 4, in parallel with the growth phenotype. Two days later, only 30% of cells had normal kDNA and 60% contained a diminished kDNA and, in the remaining 10% of flagellates, no kDNA was detected by DAPI staining. Finally, the culture appeared to stabilize between days 8 and 10, when only 10% to 15% of the flagellates retained wild-type-shaped kDNA, 50% to 60% of cells bore small kDNA, and over 30% had become akinetoplastic (Fig. 3C). Similar results were observed also in the Mge1 RNAi cell line, although the phenotype was not as severe. As shown in Fig. 3E, upon RNAi induction, the number of wild-type-looking cells was steadily going down. On day 11, the fractions of cells harboring small kDNA or lacking any trace of it eventually reached equilibrium at around 10% or 30%, respectively.

Subsequently, the RNAi cell lines depleted for mtHsp70 (days 2 and 3 postinduction) or mtHsp40 (days 6 and 8 postinduction) were examined by TEM, using a high-pressure-freezing method that allowed high-quality preservation of ultrastructural features (60). Flagellates with the "moderate" mtHsp70 phenotype were chosen in order to increase the probability of detecting any intermediate stages of the kDNA loss. As controls, wild-type cells (data
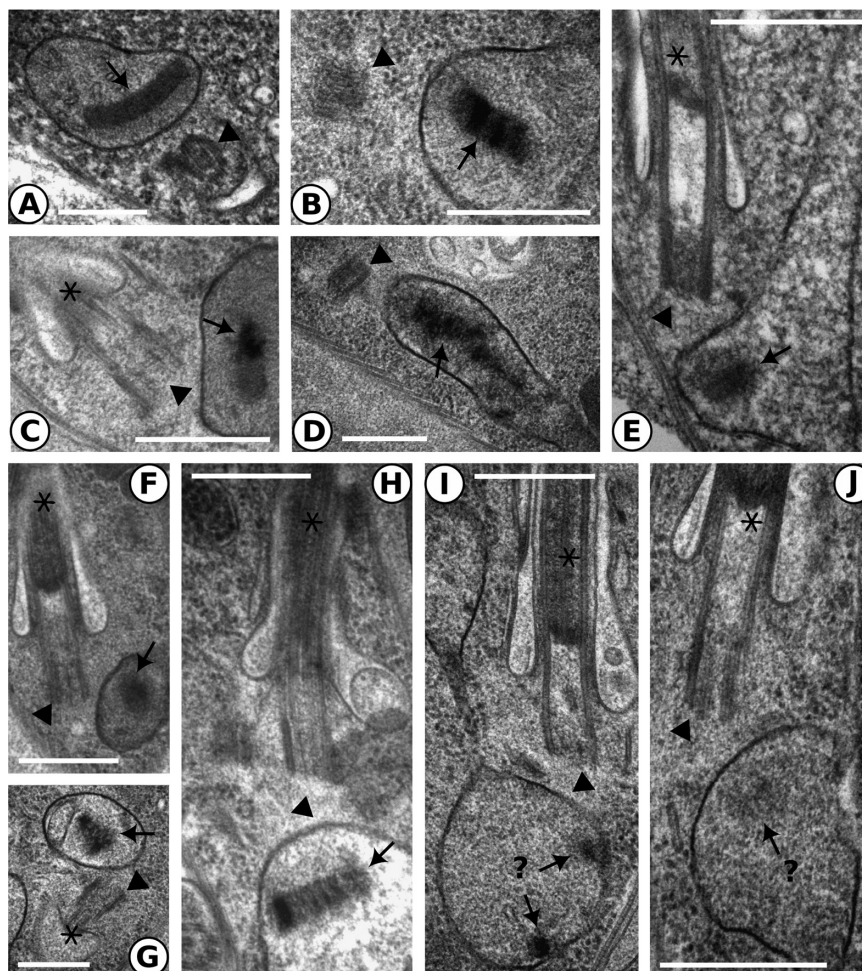
FIG 4 The ultrastructure of kDNA is severely altered in mtHsp70- and mtHsp40-depleted cells. (A) Equally electron-dense and compact kDNA disc located close to the basal body of the flagellum in an uninduced mtHsp40 RNAi cell. (B and D, F and G, H) kDNA in cells depleted for mtHsp70. On day 2 after RNAi induction, kDNA was still identifiable but already showed altered morphology (G and H). On day 3 after RNAi induction, some cells still contained an unequally electron-dense kDNA (B), while in most cells it had already lost its characteristic shape (D) and had turned into an amorphous electron-dense mass (F). (C and E, I and J) kDNA in cells depleted for mtHsp40. On day 6 after RNAi induction, the kDNA was extensively reduced in size (E); on day 8, it transformed into a small dense locus (C) or into multiple loci (I) or disappeared altogether (J). Arrows point at kDNA, arrowheads mark the basal bodies, and asterisks depict flagella. Scale bar, 500 nm.

not shown) and uninduced cells for both RNAi knockdowns were also subjected to detailed TEM analysis (Fig. 4A and Fig. 5A and B). Under normal conditions, kDNA is invariably located near the basal body of the flagellum with which it is known to be physically connected (46).

The *T. brucei* kDNA exists in the highly characteristic form of a homogenously electron-dense disk with clearly distinguishable edges (Fig. 4A and Fig. 5A and B). Depletion of either mtHsp protein resulted in progressive alteration of the kDNA morphology, gradually leading to its loss. The first observed change was the loss of even electron density across the kDNA disk (Fig. 4B), which proceeded with fading of its edges and disruption of its otherwise well-defined disk-shaped morphology with kDNA minicircles stretched taut (Fig. 4B to D, G, and H and Fig. 5E and F). These changes seemed to compromise the overall stability of the disk, as in the next stages it totally lost its structure and transformed into variously shaped but usually rounded balls of electron-dense material. The identity of the disrupted kDNA could still be convinc-

ingly confirmed due to its localization near the basal body of the flagellum and within the mt lumen (Fig. 4E and F and Fig. 5C, D, and G). In several cases, the kDNA undergoing degradation seems to have been fragmented (Fig. 4I and 5D), while this phenomenon was not observable by DAPI staining. Finally, the electron-dense material disappeared and no kDNA could be found (Fig. 4J). Interestingly, many cells were apparently able to initiate cell division even with the altered kDNA, as all described stages of kDNA loss were found in dividing cells as well (Fig. 5).

kDNA loss is a primary phenotype following depletion of mtHsp70/mtHsp40 machinery. Since mtHsp70 has so far been associated with a number of important mt processes (8, 10–14), it was necessary to establish whether the observed effect on kDNA was primary or secondary. Indeed, there are several possibilities to explain why the loss of kDNA could only be a secondary phenotype caused by the disruption of the following processes: (i) impaired protein import would deplete the kDNA replication and maintenance enzymes; (ii) overall protein stability might be com-
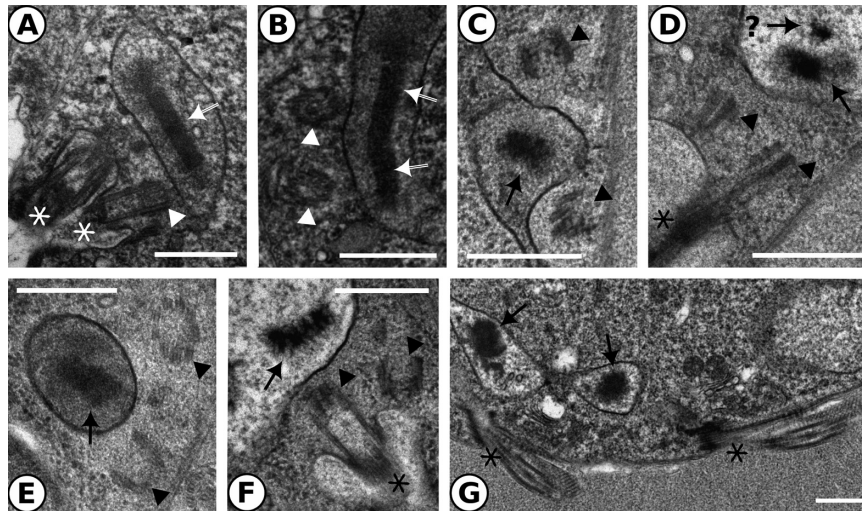
FIG 5 Cells with severely altered kDNA are able to initiate cell division. Uninduced mtHsp40 cells (A) and mtHsp70 RNAi cells (B) with normal kDNA and RNAi-induced cells (C through G) with altered kDNA morphology are shown at a division stage, exemplified by two basal bodies of their flagella. (C to G) Cells depleted for mtHsp70 (C, D, and F) (day 2 after RNAi induction) or mtHsp40 (G and E) (days 6 and 8 after RNAi induction, respectively). Arrows point at kDNA, arrowheads show the basal bodies, and asterisks depict flagella. Scale bar, 500 nm.

promised due to missing stabilizing and folding functions of the chaperones; and (iii) replication enzymes may require Fe-S clusters for their activity. Therefore, we carefully evaluated the impact of these potential secondary phenotypes. As shown in Fig. 6E, the depletion of Tim17, an essential component of the mt protein import machinery (14, 61, 62), did not cause kDNA loss. However, 4 days after RNAi induction, few cells were classified as containing smaller or no kDNA, their fraction never exceeded 10%, and there was no progressive trend to lose kDNA. Moreover, in cells ablated for Tim17, alterations in kDNA seemed to be the result of its fragmentation, as there was a higher (up to 10%) incidence of ancillary bodies (63), which emerged prior to cells with small or no kDNA (Fig. 6E). In cell lines in which other genes are targeted, ancillary bodies are exceptionally rare (data not shown).

Next, we wondered whether the depletion of mtHsp70 impacted the levels of mt matrix protein MRP2 (64), not associated with any of its putative function. In digitonin fractions obtained from mtHsp70 RNAi cells at days 3, 4, and 7 postinduction, the amount of MRP2 (64) and localization of both mtHsp70 and MRP2 proteins remained unaltered (Fig. 6I), and the same applied to the depletion of Mge1 (Fig. 6J). Finally, the fate of kDNA in trypanosomes, in which one of the core components of the essential Fe-S cluster machinery was ablated, was carefully followed. Even when analyzed for 10 days following RNAi induction, no alterations of kDNA were observed in cells depleted for IscU (65), frataxin (66), and Isd11 (67) (Fig. 6F to H), providing additional strong evidence for the kDNA-related phenotypes being a primary effect of the lack of mtHsp70. We confirmed that mtHsp70 is indeed important for Fe-S cluster synthesis in *T. brucei*, as the cluster-containing enzyme aconitase lost activity after 3 days of the presence of mtHsp70 RNAi (Fig. 6K). The activity of threonine dehydrogenase, an enzyme lacking Fe-S clusters, was used as a control. As shown in Fig. 6L, this matrix protein remained unaffected 3 days after RNAi against mtHsp70 was triggered, a time point at which the mtHsp70 target chaperone was largely depleted and kDNA structure was declining (Fig. 1B and 2B).

Depletion of the mtHsp70/mtHsp40 machinery does not disrupt the cell cycle. We wondered whether cells carrying abnormal kDNA as a consequence of mtHsp70 depletion are able to initiate and undergo cell division or whether the observed effects resulted from cell cycle disruption. Staining with DAPI, labeling with terminal deoxynucleotidyl transferase (TdT), and colocalization with the basal body-staining antibody YL1/2 were used as measures of progression through the cell cycle (68). In *T. brucei*, the earliest cytological cell cycle event is basal body duplication, a major organizing center for morphogenesis. Moreover, cells were labeled by TdT using the Tunel assay (see Materials and Methods), in which a labeled nucleotide is incorporated into the nicked and gapped (N/G) minicircles and maxicircles present solely in the replicating kDNA (69). It has been suggested that a system that retains these nicks and gaps in newly replicated minicircles is used by the parasite to ensure that each and every minicircle undergoes a single round of replication (70). It is only after all minicircles contain such nicks or gaps that these DNA strand discontinuities are filled and simultaneously sealed, leading to fast disappearance of TdT labeling, and the maternal kDNA network separates into the daughter ones (43). In an unsynchronized culture, most cells are in a 1N1K stage, which means that they contain one nucleus and one kDNA. Replication starts by duplication of the basal body, followed by the replication of kDNA. Such flagellates, labeled 1N1K* cells, contain two basal bodies and a newly replicated kDNA, which is labeled by TdT. After each kDNA minicircle and maxicircle has been replicated, the network splits, producing a 1N2K cell. Finally, the nucleus divides, and the ensuing 2N2K cell undergoes cytokinesis (59, 71). For visualization of the *T. brucei* cell cycle, see Fig. S1 in the supplemental material. As kDNA replication in *T. brucei* cannot be synchronized, unsynchronized cultures were analyzed, with cells being individually assigned to their respective categories. In each experiment, at least 250 cells were counted per time point (Fig. 7).

This experiment demonstrated that even cells with small kDNA or the akinetoplastic ones are still capable of progressing through the cell cycle. However, the growth of RNAi-induced try-
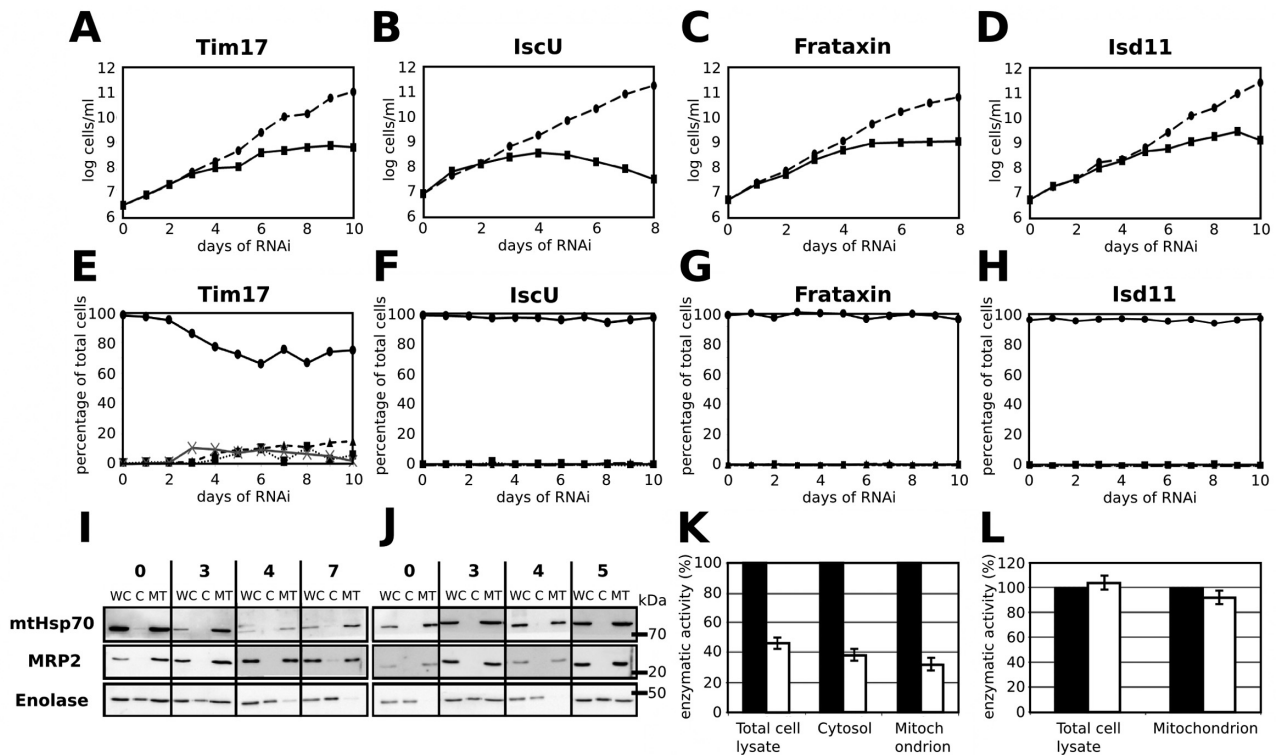
FIG 6 Defects in protein import machinery and Fe-S cluster synthesis pathway do not cause kDNA loss. (A to D) Effect of RNAi against components of the protein import or Fe-S cluster assembly on cell growth. Tim17 (A) is essential for import of proteins across the organellar double membrane; IscU (B), frataxin (C), and Isd11 (D) are essential for the synthesis of Fe-S clusters. Uninduced and RNAi-induced cells are shown by circles with a dashed line and squares with a full line, respectively. (E through H) Kinetics of kDNA changes was followed in all the RNAi cell lines described above. For each time point, 250 fixed and DAPI-stained cells were counted and multiple focal planes were checked. Cells with normal kDNA are marked by circles with a full line, while triangles with a dashed line represent cells with small kDNA and squares with a dotted line depict flagellates lacking kDNA (akinetoplastic cells). Crosses with a full grey line represent cells with 1 kDNA and 1 separate ancillary body—this cohort was present only in cells ablated for Tim17 (E). (I and J) Depletion of mtHsp70 or Mge1 did not alter the level of mt matrix protein MRP2 or affect localization of MRP2 and mtHsp70, as shown by Western blot analysis of subcellular digitonin fractions. Enolase was used as a cytosolic control. WC, whole-cell lysate; C, cytosolic fraction; MT, mt fraction. (K and L) Activity of aconitase (Fe-S cluster enzyme) was decreased whereas threonine dehydrogenase (non-Fe-S cluster enzyme) remained unaltered in a "moderate" mtHsp70 RNAi cell line on day 3 after RNAi induction, respectively. Average activities in uninduced (values arbitrarily set at 100%) and RNAi-induced cells are shown from 3 independent measurements. Black columns, uninduced cells; white columns, RNAi-induced cells.

panosomes was much slower than that of their uninduced counterparts (Fig. 1), which is why at later time points most cells existed as 1N1K (Fig. 7A and B).

This trend was more pronounced in the mtHsp40-depleted cells, which showed a gradual and less severe growth phenotype, than in the mtHsp70-depleted cells, which almost stopped dividing around the 2nd day after the addition of tetracycline (Fig. 1). The total loss of kDNA detected in this experiment (Fig. 7C and D), as well as the pattern observed in the most abundant 1N1K cell cycle stage (Fig. 7E and F), agrees with other data (Fig. 3). The detection of TdT-labeled cells in the 1N1K* configuration with diminished kDNA levels (Fig. 7G and H) means that their replication was not fully blocked. In the case of the akinetoplastic 1N2K and 2N2K cells, "2K" means that two basal bodies were detected in the absence of kDNA (Fig. 7I to L). Overall, the results of this experiment are in good correlation with those of ultrastructural analyses, which confirmed the presence of dividing cells (two basal bodies) even with altered kDNA morphology (Fig. 5).

Moreover, a gradual accumulation of cells with the unusual 2N1K configuration (only one basal body with normal, small, or no kDNA) was observed on days 4 and 8, peaking at about 10% on days 6 and 10 after RNAi induction for mtHsp70 and mtHsp40,

respectively (data not shown). However, we have noticed a peculiar difference between these two cell lines. While the basal body and kDNA are almost invariably localized at the end of the cell in cells depleted for mtHsp70, these structures are mostly localized between the two nuclei in flagellates with downregulated mtHsp40 (data not shown). This phenotype emerged quite late after RNAi induction and was therefore likely due to secondary effects.

kDNA replication and loss in mtHsp70- and mtHsp40-depleted cells. Monitoring of the kDNA replication in cells depleted for either mtHsp70 or mtHsp40 provided similar results (Fig. 8). The fate of the maxicircle and minicircle copy number was followed using Southern slot blot analysis (Fig. 8A and B), and total DNA isolated from uninduced and RNAi-induced cells was used for their quantification (Fig. 8C and D). Loss of kDNA observed by light microscopy was confirmed on the molecular level by a decline in maxicircles clearly preceding that of minicircles (Fig. 8C and D). Importantly, the copy number of both kDNA components decreased before the emergence of the growth phenotype and the complete depletion of the protein, indicating that kDNA loss is the primary phenotype.

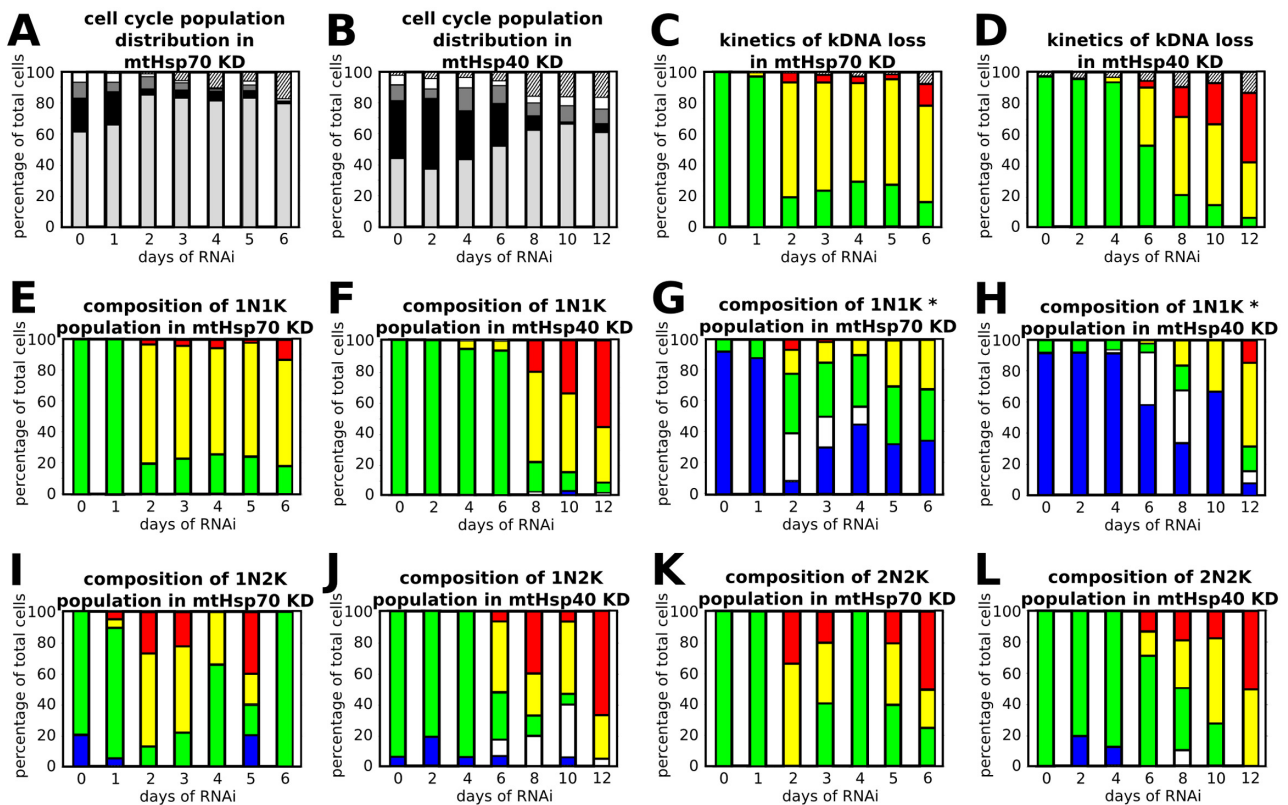In cells ablated for mtHsp70, a dramatic decline in maxicircles

FIG 7 Distribution of cell cycle stages after depletion of mtHsp70 and mtHsp40. DNA was stained with DAPI, basal bodies were visualized using specific antibodies, and TdT labeling was used to observe newly replicated kDNA to determine the cell cycle stage. Approximately 250 cells per time point were counted. (A and B) Cell cycle population distribution. Light grey, 1N1K; black, 1N1K*; dark grey, 1N2K; white, 2N2K; dashed, others. (C and D) Kinetics of kDNA loss. Green, normal kDNA; yellow, small kDNA; red, akinetoplastic cells; dashed, others. (E and F) Composition of the 1N1K population. Green, normal kDNA (TdT negative); yellow, small kDNA (TdT negative); red, akinetoplastic cells (TdT negative); blue, normal kDNA (TdT positive [replicating]); white, small kDNA (TdT positive). (G and H) Composition of the 1N1K* population. (I and J) Composition of the 1N2K population. (K and L) Composition of the 2N2K population.

to 55% and 80% of the uninduced level occurred 1 and 2 days after RNAi induction, respectively, and eventually stabilized at around 25% (Fig. 8C). The decline in minicircle levels was initially equally steep (40% were lost with 24 h of RNAi induction). However, following a short-term increase, their numbers stabilized at about 60% of the wild-type level (Fig. 8C). The impact of mtHsp40 depletion on maxicircles was even more drastic, as they were virtually undetectable by day 6, with no recovery phenotype occurring (Fig. 8D). Again, by day 2 of RNAi induction, before any alterations in growth and morphological changes of kDNA were noted, the levels of maxicircles and minicircles decreased by 50% and 15%, respectively. In the following days, in the virtual absence of maxicircles, minicircle numbers steadily declined to 50% of the uninduced levels (Fig. 8D).

Effect on minicircle replication intermediates. Minicircles are known to replicate free of the kDNA network, with the newly replicated progeny being then reattached, by the assistance of a complex dedicated machinery, into the doubling network (43). In high-resolution agarose gels run in the presence of ethidium bromide, these free minicircles can be separated into the categories of covalently closed (CC) replication precursors and nicked and gapped (N/G) replication products (Fig. 8E and F). Despite the decrease in minicircle numbers upon mtHsp70 depletion, the amounts of free CC and N/G molecules actually increased to 260% and 170%, respectively, of the levels seen with the uninduced cells

(Fig. 8G). Ablation of mtHsp40 led to a very similar phenotype, with increases in the levels of both the CC and N/G minicircle species of up to 200% and 140%, respectively (Fig. 8H). Moreover, we detected an increase in the number of oligomeric free minicircle catenanes, which were almost undetectable in the wild-type and uninduced cells (Fig. 8E and F). Another important parameter, which reflects impaired kDNA replication, is the CC-versus-N/G ratio. Indeed, in cells knocked down for either of the target genes, the ratio steadily grew, reaching a 1.6-fold increase of the ratio of the CC replication precursors to the N/G products (Fig. 8I and J).

DISCUSSION

Our goal was to understand the role of the mtHsp70/mtHsp40 machinery in mtDNA replication and maintenance. Its association with these processes was likely, since these chaperones were identified via cross-linking in the mt nucleoids of yeast and human cells (30–32). However, the possibility that such highly abundant proteins were contaminants was not rigorously excluded. In this work, mtHsp70, mtHsp40, and Mge1 localized evenly throughout the mt lumen of the single *T. brucei* mitochondrion. Given their multiple putative functions, such localization is not surprising but is partially inconsistent with the literature. mtHsp70, the only chaperone for which localization data are available from kinetoplastid parasites, was localized by immuno-
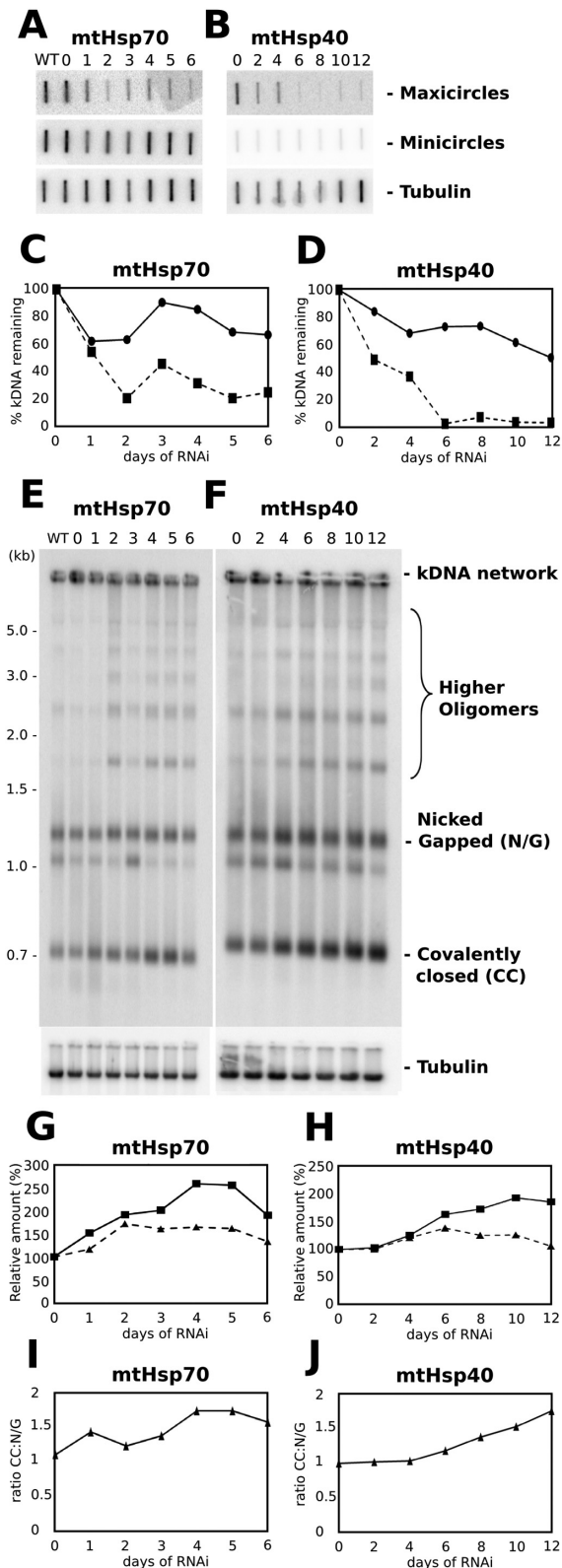
FIG 8 Analysis of kDNA loss in the absence of mtHsp70 and mtHsp40. (A and B) Southern blots with total DNA following RNAi induction of the indicated protein. Total DNA was transferred to the membrane using slot blotting. (C and D) Quantification by phosphorimaging of the maxicircle and minicircle content in panels A and B reveals a gradual decrease in the levels of *(Continued)*

fluorescence microscopy within the kDNA network of *Trypanosoma cruzi* (34) and *Crithidia fasciculata* (35). Furthermore, the same antibody generated against *T. cruzi* mtHsp70 selectively labeled kDNA in *T. brucei* as well, while in its akinetoplastic strain, the whole mitochondrion was stained (72). However, results from *Leishmania major* (73) and other *Leishmania* spp. are fully consistent with our observations, with mtHsp70 distributed throughout the organelle (73, 74). So far, there is no evidence for the mtHsp70/mtHsp40 machinery being subjected to dynamic localization changes during the cell cycle of *T. brucei*. Therefore, we propose that the *T. cruzi* antibody that labels the kDNA disk recognizes only a subpopulation of the mtHsp70 protein that is specifically localized within and/or in the close proximity of this structure. Since mtHsp70 and some other kDNA-binding proteins were recently found to be arginine methylated in *T. brucei* (75), a plausible scenario is that the anti-*T. cruzi* mtHsp70 antibody specifically recognizes only mtHsp70 with this posttranslational modification. Furthermore, it is tempting to speculate that methylation might serve as a kDNA-targeting signal. Indeed, the yeast data are consistent with this interpretation, as just a portion of Ssc1 is associated with the mt nucleoids (33).

Chaperones of the 40-kDa family (Table 1) also localize to the mt nucleoid in yeast and human cells (33, 38), and Mdj1 and all three *E. coli* DnaJ proteins were shown to directly bind DNA, this binding being disrupted by the addition of protein substrate (29, 33). Taken together, these data indicate that mtHsp40 is predominantly localized in the nucleoid of *E. coli*, yeast, and human cells, where it performs its primary function; it is only under conditions in which protein substrates become available, such as upon a heat shock, that mtHsp40 dissociates to perform its chaperone function. So far, any possible DNA binding properties of their *T. brucei* mtHsp40 homologue, which localizes throughout the mt lumen, remain to be determined. In yeast and mammals, the mt nucleoids are more or less evenly dispersed throughout the organellar matrix, making the chaperones available when needed. However, the *T. brucei* kDNA network is invariably present in the anterior parabasal region of a single tubular mitochondrion, and hence a strict DNA binding of the chaperones would be an impediment to their availability throughout the organelle in case of need. Therefore, uniform distribution of mtHsp40, with only its fraction bound to the kDNA, seems to be a more suitable solution for the flagellate.

To further dissect the relationships between the mtHsp70/mtHsp40 machinery and mtDNA, we took advantage of unique kDNA features, such as its exceptional size, catenated structure,

Figure Legend Continued

kDNA maxicircles (dashed line with squares) and minicircles (full line with circles) after depletion of the indicated protein. Values were normalized against α-tubulin used as a control. (E and F) Southern blot analysis of free minicircle replication intermediates following RNAi induction of the indicated protein. Total DNA was separated on a 1.5% agarose gel in the presence of ethidium bromide and transferred to a nylon membrane, which was first probed for minicircles and then stripped and reprobed with the α-tubulin probe. (G and H) Free minicircle replication intermediates from panels E and F quantified by phosphorimaging. Both covalently closed (CC) (full line with squares) and nicked/gapped (N/G) (dashed line with triangles) minicircle replication intermediates increased in numbers after depletion of mtHsp70 or mtHsp40. Values were normalized against the α-tubulin control. (I and J) Relative abundances of free minicircle replication intermediates after depletion of the indicated protein. Higher abundance of the CC replication precursors compared to the N/G replication product indicates impaired minicircle replication.

two types of DNA molecules, and replication only once per cell cycle (41, 42). These features provide a robust platform for phenotypic analyses of these organellar chaperones and allow reliable quantification of the data. Depletion of mtHsp70, mtHsp40, and Mge1 invariably led to the shrinkage and eventual loss of kDNA. However, in cells ablated for Mge1, the delayed kDNA loss was likely secondary, caused by nonfunctional mtHsp70. The exceptionally compact packaging of the kDNA disk allowed us to monitor its severely compromised ultrastructure upon downregulation of mtHsp70 or mtHsp40. The initial loss of homogeneity of the disk resembles a phenotype triggered by the depletion of helicase Pif8, which was assigned a role in kDNA maintenance (76). Several days after the induction of RNAi targeting of the studied chaperones, the kDNA disk shrinks into an irregularly shaped electron-dense structure, which eventually disappears. This phenotype is highly reminiscent of the one associated with the ablation of p38, an origin-binding protein involved in kDNA replication (53).

Although the pLew100-derived mtHsp70 RNAi cells exhibited a stronger growth phenotype, there was no substantial difference between the "severe" and "moderate" cell lines according to the results of analysis of the pattern of kDNA loss. We interpret this result as a consequence of the capacity of the RNAi-induced trypanosomes to still undergo at least two to three cell divisions before a diminution of kDNA levels can be observed. This result also suggests that the loss of kDNA may be due to dysfunctional kDNA replication rather than to degradation. Since the flagellates are still able to progress through the cell cycle despite severely altered and shrinking kDNA, its loss seems to be the primary consequence of depletion of mtHsp70 and not a secondary effect caused by cell cycle disruption.

The reduction in the copy number appeared to be more pronounced in the case of maxicircles than of minicircles. We propose that it is due to the highly conserved function of mtHsp70 and mtHsp40 from prokaryotes to mitochondria, as, in the kDNA network, maxicircles are true homologues of mtDNA. However, the dramatic ultrastructural changes of the kDNA disk eventually leading to its complete disappearance must be a consequence of the depletion of minicircles, since the dyskinetoplastic trypanosomes, which lost all maxicircles but retained minicircles, retained a kDNA disk indistinguishable in size and ultrastructure from its wild-type form (77). This interpretation is further supported by functional studies of the Pif2 helicase, the depletion of which causes selective loss of maxicircles, and yet the size and morphology of the kDNA disk remain unaltered (78).

Since minicircles represent the bulk of the kDNA network, its shrinkage is inevitably reflected in the decline of their copy number. However, if the reattachment of postreplication minicircles is compromised, free replication intermediates may accumulate, an effect we actually observed in cells depleted for the mtHsp70/mtHsp40 machinery. A steep increase in the numbers of covalently closed replication precursors in parallel with a less dramatic increase in the numbers of the nicked and gapped species would be reflected in their growth ratio, direct evidence of the impaired minicircle replication seen in both RNAi cell lines (Fig. 8). Indeed, shifts in the monitored minicircle species are compatible with the failure of minicircles released from the network to undergo replication, resulting in progressive shrinkage of the kDNA disk and the accumulation of free minicircles. It is worth noting that, in the first days of RNAi induction, minicircle replication was not com-

pletely inhibited but instead slowed down, since newly replicated DNA was detected via TdT labeling in the diminishing kDNA networks.

Overall, the consequences for kDNA of the mtHsp70 and mtHsp40 depletion are comparable to those of other kDNA replication proteins described in the *T. brucei* model system. Comparison of the obtained phenotypes in terms of kDNA loss, impaired minicircle replication, and their recatenation, as well as the strong decline in maxicircles, led to the identification of proteins that may function at the same step of kDNA replication and may be potential partners of these chaperones. A common feature of the proteins identified so far—DNA primase 1 (57), mtDNA polymerases IC (54) and ID (55), and kDNA origin of replication-binding protein p38 (53)—is that they all function in the beginning of kDNA replication. The latter protein may somehow facilitate priming, as it was shown not only to bind kDNA but also to stabilize mtRNA (79). The observation of similar effects on kDNA upon the depletion of either mtHsp70 or mtHsp40 supports the hypothesis that the two proteins cooperate with each other and participate in kDNA replication and maintenance, yet the complexity of these processes in *T. brucei*, supported by uniquely numerous primases (57, 80), ligases (81), helicases (76, 78, 82, 83), and DNA polymerases (54, 84, 85), imposes limits to direct comparisons.

Depletions of mtHsp40 and kDNA replication enzymes result in very similar growth phenotypes (53–57). However, the downregulation of mtHsp70 causes a significantly stronger growth effect, which is likely caused by a combined effect on several processes disrupted in parallel, such as general chaperone function and folding (7–9), Fe-S cluster biogenesis (10, 11), and mt protein import (12). Therefore, it was necessary to address the issue of whether kDNA loss is truly the primary phenotype caused by the lack of this multifunctional protein. Due to the general importance of the chaperone function, to ensure proper protein folding, a typical cell has not relied within its mitochondria on a single protein but has evolved a complex chaperone-protease network (86). While under normal conditions, the chaperone function is dispensable, under heat shock conditions, mtHsp70 and mtHsp40 are required for proper mtDNA polymerase activity (36, 37). Similarly, when grown at standard temperature, growth retardation of a yeast mutant defective in Ssc1 is restored if its importation, but not its folding functions, is corrected (9).

By evaluating the impact of mtHsp70 depletion on various processes, including Fe-S cluster assembly, we showed that threonine dehydrogenase, an enzyme independent of clusters, remained active, whereas the activity of the cluster-containing aconitase dropped significantly. However, downregulation of any of the three screened key components of the Fe-S cluster assembly pathway (65–67) had no impact on the kDNA content and structure, although numerous DNA replication proteins are known to require clusters for their activity (87, 88). Similarly, the impairment of mt protein import via the ablation of Tim17 (14, 61, 62) did not trigger the loss of kDNA. Hence, the observed drastic alterations of kDNA in trypanosomes depleted for any of the studied mt chaperones are tightly associated with their function in kDNA replication and maintenance. Our report is also relevant from the evolutionary point of view. So far, similar analyses have been performed only in members of the supergroup *Opisthokonta*, while *T. brucei* is a member of the likely ancestral supergroup *Excavata*. Hence, this report confirms the very high conservation

and importance of mtHsp70 in mtDNA-related functions in eukaryotes in general.

Based on the interpretation of our results and the analysis of the existing literature, we propose the following hypothesis as to how mtHsp40/mtHsp70 machinery functions in the mitochondrion. MtHsp40 binds to the organellar DNA and recruits mtHsp70 to it. With the support of Mge1, these proteins then remodel and activate the mtDNA replication machinery. In the first step, a protein with specific binding to the origin of replication is recruited which functions as the DnaA protein in prokaryotes. This protein enables helicase to unwind the DNA and facilitate loading of primase and, subsequently, mtDNA polymerase. From the available data, we cannot determine the exact step in which the chaperones are involved and or rule out the possibility that they are required for the whole process of replication initiation. In summary, our results reveal for the first time that the mtHsp70/mtHsp40 machinery retained its role in DNA replication and maintenance acquired by their bacterial ancestors.

MATERIALS AND METHODS

Cell culture and generation of RNAi and PTP-tagged cell lines. Procyclic *T. brucei* strains 29 to 13 were grown in SDM-79 medium containing 10% fetal bovine serum, 15 μg·ml^{-1} geneticin, and 50 μg·ml^{-1} hygromycin. For RNAi, gene fragments of mtHsp70 (Tb927.6.3740, Tb927.6.3750, and Tb927.6.3800), mtHsp40 (Tb927.9.12730), and Mge1 (Tb927.6.2170) were PCR amplified from the *T. brucei* genomic DNA using primers listed in Table S1 in the supplemental material. In case of mtHsp70, transcripts of all three mtHsp70 genes present in the genome were targeted. The PCR amplicon was gel purified, digested with indicated restriction enzymes (see Table S1), and ligated into the p2T7-177 vector predigested with the same enzymes. All plasmids were linearized using NotI, electroporated, and selected as described elsewhere (64). RNAi cell lines with targeted IscU, frataxin, Isd11, or Tim17 have been described previously (60, 64–66). The "severe" phenotype mtHsp70 cell lines were obtained by electroporating the corresponding gene fragment within the pLew100 vector into the *T. brucei* 427 SiMP single-marker cell line (14). RNAi was induced by the addition of tetracycline (1 μg·ml^{-1}) to the growth medium, and cell densities were measured using a Beckman Coulter Z2 counter every 24 h over a period of 7 to 12 days after RNAi induction.

For integration of the tandem affinity purification PTP tag into the endogenous gene locus, the amplicon was ligated into the pC-PTP-Puro vector (89) (for primers, see Table S1 in the supplemental material). Prior to electroporation, vectors containing the mtHsp40, mtHsp70, or Mge1 gene were linearized within the inserted gene sequence with restriction enzyme SphI, BlpI, or XhoI, respectively, and puromycin was used as a selection marker. In the case of mtHsp40, RNAi cells for the corresponding gene were used as a parental cell line.

Expression of recombinant TbMge1, antibody generation, and Western blot analysis. The PCR amplicon containing the full-size TbMge1 gene was gel purified and cloned into the pET/100D-TOPO expression vector (Invitrogen). The resulting expression plasmid encoding His$_6$-tagged Mge1 was transformed into the *E. coli* BL21(DE3) Star strain (Novagen). Soluble protein was obtained from induced bacterial cells (incubation at 37°C for 3 h and induction with 0.5 μm IPTG [isopropyl-β-D-thiogalactopyranoside]) using ProBond nickel-chelating resin (Invitrogen). Polyclonal antibodies against TbMge1 were prepared by immunizing a rabbit following an immunization protocol described elsewhere (90).

For Western blot analysis, cells were harvested by centrifugation and lysed in hot Laemmli sample buffer. Lysates equivalent to 5×10^6 cells were separated by 12% SDS-PAGE, blotted, and probed with the following antibodies: monoclonal antibody against mtHsp70 (58), commercial anti-protein A antibody (Sigma-Aldrich), and polyclonal antibodies against TbMge1 (this work), MRP2 (64), Nfs1 (65), and enolase (kindly

provided by P. A. M. Michels). The antibodies were used at 1:1,000 dilutions, except the anti-protein A antibody, which was used at 1:5,000. The secondary anti-rabbit IgG antibodies (1:1,000) and anti-rat IgG antibodies (1:1,000) coupled to alkaline phosphatase or horseradish peroxidase were visualized according to the manufacturer's protocols using Clarity Western ECL substrate (Bio-Rad).

Subcellular fractionation and enzyme activity measurements. The cytosolic and mt fractions were acquired by a digitonin fractionation procedure described elsewhere (65). All enzymatic activities were measured spectrophotometrically as described previously (66). Briefly, in both subcellular compartments (cytosol and mitochondrion), aconitase was measured at 240 nm via the production of *cis*-aconitate from isocitrate. Activity of threonine dehydrogenase was established at 340 nm as the rate of NAD$^+$ reduction.

Immunofluorescence microscopy. Cells in logarithmic phase were harvested at $1,000 \times g$ for 5 min, resuspended in phosphate-buffered saline (PBS), and adhered to poly-L-lysine (1:10)-coated slides for 5 min. They were fixed in 4% paraformaldehyde for 5 min and washed three times (for 5 min each time) in PBS containing 0.1 M glycine (pH 7.4), followed by permeabilization with methanol overnight at −20°C. Next, cells were rehydrated in PBS 3 times for 5 min each time, followed by blocking in PBS containing 1% bovine serum albumin (BSA) and 0.1% Tween 20 for 60 min. Afterward, incubation in PBS containing 1% BSA with anti-protein A antibodies (Sigma), anti-mtHsp70 mouse monoclonal antibodies (58), or rat monoclonal antibody YL1/2 (Abcam) followed for 60 min, at dilutions of 1:5,000, 1:100, or 1:3,000, respectively. Cells were then washed 3 times in PBS containing 0.1% Tween 20 and incubated for 60 min with secondary goat anti-rabbit antibody Alexa Fluor 594 or goat anti-rat antibody Alexa Fluor 488, both diluted 1:250 in PBS containing 1% BSA. DNA was stained with 3 μg/ml DAPI, and slides were washed 3 times in PBS prior to mounting in Vectashield (Vector Laboratories). When Mitotracker staining was performed, cells were incubated in a medium supplemented with 200 nM Mitotracker Red CMX (Molecular Probes) for 20 min prior to harvesting.

For TdT labeling, cells were incubated for 20 min at room temperature in 1× TdT reaction buffer (Roche Applied Science) containing 2 mM CoCl$_2$ after permeabilization with methanol and rehydration in PBS. Next, cells were labeled for 60 min at room temperature in a 20-μl volume of reaction mixture (1× TdT reaction buffer, 2 mM CoCl$_2$, 10 μM dATP, 5 μM Alexa Fluor 488-dUTP, and 10 U of TdT), which was stopped by the addition of 2× SSC (1× SSC is 0.15 M NaCl plus 0.015 M sodium citrate). Finally, after 3 washes in PBS, slides were processed for immunolocalization as described above.

Transmission electron microscopy. The pellet of cultured cells was mixed with a drop of 20% BSA and centrifuged at $1,000 \times g$ for 30 s. A small drop of about 1 μl containing a compact cell pellet was transferred into a gold-plated flat specimen carrier (Leica) (thickness, 0.5 mm; diameter, 1.2 mm; depth, 200 μm) and frozen using a high-pressure EM PACT2 freezer (Leica). After freezing, the samples were transferred into special containers filled with a freeze substitution medium (2% OsO$_4$–100% acetone) precooled to −90°C by liquid nitrogen in an AFS device freeze-substitution system (Leica). Samples were freeze substituted starting at −90°C for 96 h, followed by warming at 5°C per h, for 14 h, to −20°C. After 24 h at −20°C, samples were warmed using a step of 3°C per h for the following 8 h. After 18 h at 4°C, the procedure finished and cells were rinsed 3 times in 100% acetone at room temperature and infiltrated in a mixture of acetone/resin Epon (SPI) media (2:1, 1:1, and 1:2 for 1 h at each step). After an overnight incubation in pure Epon resin, specimens were embedded in fresh resin and polymerized at 62°C for 48 h. Ultrathin sections (thickness, 70 to 90 nm) were cut using an ultramicrotome (UCT; Leica) and collected on copper grids. The grids were contrasted in ethanol-containing uranyl acetate and lead citrate and observed in a JEOL 1010 TEM at an accelerating voltage of 80 kV. Images were captured using a Mega view III charge-coupled-device (CCD) camera (SIS).

DNA isolation and Southern blot analysis. Total DNA was isolated from 1×10^8 cells using Purgene core kit B (Qiagene). For Southern blot analysis of kDNA minicircles and maxicircles, total DNA was subjected to Southern blot or slot blot analysis. Briefly, 1 vol of DNA (from approximately 1×10^6 cells) was denatured by the addition of 1 vol of 0.3 N HCl for 10 min and then neutralized by the addition of 10 vol of 0.4 N NaOH and 25 mM EDTA. Afterward, the sample was applied to the membrane using a dot blotter and washed by 2 vol of $20\times$ SSC. A UV cross-linked membrane was used for hybridization.

For analysis of free minicircle replication intermediates, total DNA was fractionated on a 1.5% agarose gel for 16 h at 2.4 $V \cdot cm^{-1}$ with 1.0 $mg \cdot ml^{-1}$ ethidium bromide in the gel and Tris-borate-EDTA running buffer (the buffer was recirculated). Fractionated DNA was processed using standard depurination, denaturation, and neutralization treatments, transferred to a GeneScreen Plus membrane using capillary transfer, and then subjected to UV cross-linking. Membranes were probed with maxicircle-, minicircle-, and α-tubulin-specific random primed ^{32}P-radiolabeled PCR products. The primers that were used are listed in Table S1 in the supplemental material. Genomic DNA was used as a template for the maxicircle and tubulin probes, while the minicircle probe was amplified from the pJN6 vector containing the full-length *T. equiperdum* minicircle sequence (91). Hybridizations with the maxicircle, minicircle, or tubulin probes were carried out overnight at 42°C in 50% formamide–$5\times$ SSC–10% dextran sulfate–1% SDS–$1\times$ Denhardt's solution–0.2 mg/ml salmon sperm DNA. Blots were washed twice for 5 min at 42°C consecutively in each of the following solutions: $2\times$ SSC, $1\times$ SSC, and $0.1\times$ SSC plus 0.1% SDS. Stripping was performed by incubating the membrane in boiling 0.1% SDS for 10 min. Images were obtained by the use of a Typhoon 9210 Molecular Dynamics PhosphorImager (GE Healthcare), and the results were quantified in ImageJ software and normalized against the tubulin signal.

SUPPLEMENTAL MATERIAL

Supplemental material for this article may be found at http://mbio.asm.org/lookup/suppl/doi:10.1128/mBio.02425-14/-/DCSupplemental.

Figure S1, JPG file, 0.4 MB.
Table S1, DOCX file, 0.01 MB.

ACKNOWLEDGMENTS

REFERENCES

1. **Tyynismaa H, Mjosund KP, Wanrooij S, Lappalainen I, Ylikallio E, Jalanko A, Spelbrink JN, Paetau A, Suomalainen A.** 2005. Mutant mitochondrial helicase twinkle causes multiple mtDNA deletions and a late-onset mitochondrial disease in mice. Proc Natl Acad Sci U S A **102:**17687–17692. http://dx.doi.org/10.1073/pnas.0505551102.

2. **Goffart S, Cooper HM, Tyynismaa H, Wanrooij S, Suomalainen A, Spelbrink JN.** 2009. Twinkle mutations associated with autosomal dominant progressive external ophthalmoplegia lead to impaired helicase function and in vivo mtDNA replication stalling. Hum Mol Genet **18:**328–340. http://dx.doi.org/10.1093/hmg/ddn359.

3. **Calvo SE, Mootha VK.** 2010. The mitochondrial proteome and human disease. Annu Rev Genomics Hum Genet **11:**25–44. http://dx.doi.org/10.1146/annurev-genom-082509-141720.

4. **Copeland WC.** 2008. Inherited mitochondrial diseases of DNA replication. Annu Rev Med **59:**131–146. http://dx.doi.org/10.1146/annurev.med.59.053006.104646.

5. **El-Hattab AW, Scaglia F.** 2013. Mitochondrial DNA depletion syndromes: review and updates of genetic basis, manifestations, and therapeutic options. Neurotherapeutics **10:**186–198. http://dx.doi.org/10.1007/s13311-013-0177-6.

6. **Falah M, Gupta RS.** 1994. Cloning of the hsp70 (dnaK) genes from *Rhizobium meliloti* and *Pseudomonas cepacia*: phylogenetic analyses of mitochondrial origin based on a highly conserved protein sequence. J Bacteriol **176:**7748–7753.

7. **Folgueira C, Requena JM.** 2007. A postgenomic view of the heat shock proteins in kinetoplastids. FEMS Microbiol Rev **31:**359–377. http://dx.doi.org/10.1111/j.1574-6976.2007.00069.x.

8. **Voos W, Röttgers K.** 2002. Molecular chaperones as essential mediators of mitochondrial biogenesis. Biochim Biophys Acta **1592:**51–62. http://dx.doi.org/10.1016/S0167-4889(02)00264-1.

9. **Liu Q, Krzewska J, Liberek K, Craig EA.** 2001. Mitochondrial Hsp70 Ssc1: role in protein folding. J Biol Chem **276:**6112–6118. http://dx.doi.org/10.1074/jbc.M009519200.

10. **Dutkiewicz R, Schilke B, Knieszner H, Walter W, Craig EA, Marszalek J.** 2003. Ssq1, a mitochondrial Hsp70 involved in iron-sulfur (Fe/S) center biogenesis. Similarities to and differences from its bacterial counterpart. J Biol Chem **278:**29719–29727. http://dx.doi.org/10.1074/jbc.M303527200.

11. **Lill R, Mühlenhoff U.** 2008. Maturation of iron-sulfur proteins in eukaryotes: mechanisms, connected processes, and diseases. Annu Rev Biochem **77:**669–700. http://dx.doi.org/10.1146/annurev.biochem.76.052705.162653.

12. **Liu Q, D'Silva P, Walter W, Marszalek J, Craig EA.** 2003. Regulated cycling of mitochondrial Hsp70 at the protein import channel. Science **300:**139–141. http://dx.doi.org/10.1126/science.1083379.

13. **Schneider A, Bursać D, Lithgow T.** 2008. The direct route: a simplified pathway for protein import into the mitochondrion of trypanosomes. Trends Cell Biol **18:**12–18. http://dx.doi.org/10.1016/j.tcb.2007.09.009.

14. **Tschopp F, Charrière F, Schneider A.** 2011. In vivo study in *Trypanosoma brucei* links mitochondrial transfer RNA import to mitochondrial protein import. EMBO Rep **12:**825–832. http://dx.doi.org/10.1038/embor.2011.111.

15. **Alfonzo JD, Söll D.** 2009. Mitochondrial tRNA import—the challenge to understand has just begun. Biol Chem **390:**717–722. http://dx.doi.org/10.1515/BC.2009.101.

16. **Szabo A, Langer T, Schröder H, Flanagan J, Bukau B, Hartl FU.** 1994. The ATP hydrolysis-dependent reaction cycle of the *Escherichia coli* Hsp70 system DnaK, DnaJ, and GrpE. Proc Natl Acad Sci U S A **91:**10345–10349. http://dx.doi.org/10.1073/pnas.91.22.10345.

17. **Miao B, Davis JE, Craig EA.** 1997. Mge1 functions as a nucleotide release factor for Ssc1, a mitochondrial Hsp70 of *Saccharomyces cerevisiae*. J Mol Biol **265:**541–552. http://dx.doi.org/10.1006/jmbi.1996.0762.

18. **Schmidt S, Strub A, Röttgers K, Zufall N, Voos W.** 2001. The two mitochondrial heat shock proteins 70, Ssc1 and Ssq1, compete for the cochaperone Mge1. J Mol Biol **313:**13–26. http://dx.doi.org/10.1006/jmbi.2001.5013.

19. **Slutsky-Leiderman O, Marom M, Iosefson O, Levy R, Maoz S, Azem A.** 2007. The interplay between components of the mitochondrial protein translocation motor studied using purified components. J Biol Chem **282:**33935–33942. http://dx.doi.org/10.1074/jbc.M704435200.

20. **Fan CY, Lee S, Cyr DM.** 2003. Mechanisms for regulation of Hsp70 function by Hsp40. Cell Stress Chaperones **8:**309–316. http://dx.doi.org/10.1379/1466-1268(2003)008<0309:MFROHF>2.0.CO;2.

21. **Dudek J, Rehling P, van der Laan M.** 2013. Mitochondrial protein import: common principles and physiological networks. Biochim Biophys Acta **1833:**274–285. http://dx.doi.org/10.1016/j.bbamcr.2012.05.028.

22. **Louw CA, Ludewig MH, Mayer J, Blatch GL.** 2010. The Hsp70 chaperones of the Tritryps are characterized by unusual features and novel members. Parasitol Int **59:**497–505. http://dx.doi.org/10.1016/j.parint.2010.08.008.

23. **Uzarska MA, Dutkiewicz R, Freibert SA, Lill R, Mühlenhoff U.** 2013. The mitochondrial Hsp70 chaperone Ssq1 facilitates Fe/S cluster transfer from Isu1 to Grx5 by complex formation. Mol Biol Cell **24:**1830–1841. http://dx.doi.org/10.1091/mbc.E12-09-0644.

24. **Sakasegawa Y, Hachiya NS, Tsukita S, Kaneko K.** 2003. Ecm10p localizes in yeast mitochondrial nucleoids and its overexpression induces extensive

mitochondrial DNA aggregations. Biochem Biophys Res Commun **309**: 217–221. http://dx.doi.org/10.1016/S0006-291X(03)01548-1.

25. **Baumann F, Milisav I, Neupert W, Herrmann JM.** 2000. Ecm10, a novel hsp70 homolog in the mitochondrial matrix of the yeast *Saccharomyces cerevisiae*. FEBS Lett **487**:307–312. http://dx.doi.org/10.1016/S0014-5793(00)02364-4.

26. **Sakakibara Y.** 1988. The dnaK gene of *Escherichia coli* functions in initiation of chromosome replication. J Bacteriol **170**:972–979.

27. **Sozhamannan S, Chattoraj DK.** 1993. Heat shock proteins DnaJ, DnaK, and GrpE stimulate P1 plasmid replication by promoting initiator binding to the origin. J Bacteriol **175**:3546–3555.

28. **Hoffmann HJ, Lyman SK, Lu C, Petit MA, Echols H.** 1992. Activity of the Hsp70 chaperone complex—DnaK, DnaJ, and GrpE—in initiating phage lambda DNA replication by sequestering and releasing lambda P protein. Proc Natl Acad Sci U S A **89**:12108–12111. http://dx.doi.org/10.1073/pnas.89.24.12108.

29. **Gur E, Katz C, Ron EZ.** 2005. All three J-domain proteins of the *Escherichia coli* DnaK chaperone machinery are DNA binding proteins. FEBS Lett **579**:1935–1939. http://dx.doi.org/10.1016/j.febslet.2005.01.084.

30. **Nosek J, Tomáška L, Bolotin-Fukuhara M, Miyakawa I.** 2006. Mitochondrial chromosome structure: an insight from analysis of complete yeast genomes. FEMS Yeast Res **6**:356–370. http://dx.doi.org/10.1111/j.1567-1364.2005.00016.x.

31. **Wang Y, Bogenhagen DF.** 2006. Human mitochondrial DNA nucleoids are linked to protein folding machinery and metabolic enzymes at the mitochondrial inner membrane. J Biol Chem **281**:25791–25802. http://dx.doi.org/10.1074/jbc.M604501200.

32. **Bogenhagen DF, Rousseau D, Burke S.** 2008. The layered structure of human mitochondrial DNA nucleoids. J Biol Chem **283**:3665–3675. http://dx.doi.org/10.1074/jbc.M708444200.

33. **Ciesielski GL, Plotka M, Manicki M, Schilke BA, Dutkiewicz R, Sahi C, Marszalek J, Craig EA.** 2013. Nucleoid localization of Hsp40 Mdj1 is important for its function in maintenance of mitochondrial DNA. Biochim Biophys Acta **1833**:2233–2243. http://dx.doi.org/10.1016/j.bbamcr.2013.05.012.

34. **Engman DM, Kirchhoff LV, Donelson JE.** 1989. Molecular cloning of mtp70, a mitochondrial member of the hsp70 family. Mol Cell Biol **9**:5163–5168.

35. **Effron PN, Torri AF, Engman DM, Donelson JE, Englund PT.** 1993. A mitochondrial heat shock protein from *Crithidia fasciculata*. Mol Biochem Parasitol **59**:191–200. http://dx.doi.org/10.1016/0166-6851(93)90217-L.

36. **Duchniewicz M, Germaniuk A, Westermann B, Neupert W, Schwarz E, Marszalek J.** 1999. Dual role of the mitochondrial chaperone Mdj1p in inheritance of mitochondrial DNA in yeast. Mol Cell Biol **19**:8201–8210.

37. **Germaniuk A, Liberek K, Marszalek J.** 2002. A bichaperone (Hsp70-Hsp78) system restores mitochondrial DNA synthesis following thermal inactivation of Mip1p polymerase. J Biol Chem **277**:27801–27808. http://dx.doi.org/10.1074/jbc.M201756200.

38. **Lu B, Garrido N, Spelbrink JN, Suzuki CK.** 2006. Tid1 isoforms are mitochondrial DnaJ-like chaperones with unique carboxyl termini that determine cytosolic fate. J Biol Chem **281**:13150–13158. http://dx.doi.org/10.1074/jbc.M509179200.

39. **Hayashi M, Imanaka-Yoshida K, Yoshida T, Wood M, Fearns C, Tatake RJ, Lee JD.** 2006. A crucial role of mitochondrial Hsp40 in preventing dilated cardiomyopathy. Nat Med **12**:128–132. http://dx.doi.org/10.1038/nm1327.

40. **Barrett MP, Burchmore RJ, Stich A, Lazzari JO, Frasch AC, Cazzulo JJ, Krishna S.** 2003. The trypanosomiases. Lancet **362**:1469–1480. http://dx.doi.org/10.1016/S0140-6736(03)14694-6.

41. **Englund PT.** 1978. The replication of kinetoplast DNA networks in *Crithidia fasciculata*. Cell **14**:157–168. http://dx.doi.org/10.1016/0092-8674(78)90310-0.

42. **Woodward R, Gull K.** 1990. Timing of nuclear and kinetoplast DNA replication and early morphological events in the cell cycle of *Trypanosoma brucei*. J Cell Sci **95**:49–57.

43. **Jensen RE, Englund PT.** 2012. Network news: the replication of kinetoplast DNA. Annu Rev Microbiol **66**:473–491. http://dx.doi.org/10.1146/annurev-micro-092611-150057.

44. **Hashimi H, Zimmer SL, Ammerman ML, Read LK, Lukeš J.** 2013. Dual core processing: MRB1 is an emerging kinetoplast RNA editing complex. Trends Parasitol **29**:91–99. http://dx.doi.org/10.1016/j.pt.2012.11.005.

45. **Verner Z, Basu S, Benz C, Dixit S, Dobáková E, Faktorová D, Hashimi**

H, Horáková E, Huang Z, Paris Z, Pena-Diaz P, Ridlon L, Týč J, Wildridge D, Zíková A, Lukeš J. The malleable mitochondrion of *Trypanosoma brucei*. Int Rev Cell Mol Biol, in press.

46. **Ogbadoyi EO, Robinson DR, Gull K.** 2003. A high-order transmembrane structural linkage is responsible for mitochondrial genome positioning and segregation by flagellar basal bodies in trypanosomes. Mol Biol Cell **14**:1769–1779. http://dx.doi.org/10.1091/mbc.E02-08-0525.

47. **Berriman M, Ghedin E, Hertz-Fowler C, Blandin G, Renauld H, Bartholomeu DC, Lennard NJ, Caler E, Hamlin NE, Haas B, Böhme U, Hannick L, Aslett MA, Shallom J, Marcello L, Hou L, Wickstead B, Alsmark UC, Arrowsmith C, Atkin RJ, Barron AJ, Bringaud F, Brooks K, Carrington M, Cherevach I, Chillingworth TJ, Churcher C, Clark LN, Corton CH, Cronin A, Davies RM, Doggett J, Djikeng A, Feldblyum T, Field MC, Fraser A, Goodhead I, Hance Z, Harper D, Harris BR, Hauser H, Hostetler J, Ivens A, Jagels K, Johnson D, Johnson J, Jones K, Kerhornou AX, Koo H, Larke N, et al.** 2005. The genome of the African trypanosome *Trypanosoma brucei*. Science **309**:416–422. http://dx.doi.org/10.1126/science.1112642.

48. **Aslett M, Aurrecoechea C, Berriman M, Brestelli J, Brunk BP, Carrington M, Depledge DP, Fischer S, Gajria B, Gao X, Gardner MJ, Gingle A, Grant G, Harb OS, Heiges M, Hertz-Fowler C, Houston R, Innamorato F, Iodice J, Kissinger JC, Kraemer E, Li W, Logan FJ, Miller JA, Mitra S, Myler PJ, Nayak V, Pennington C, Phan I, Pinney DF, Ramasamy G, Rogers MB, Roos DS, Ross C, Sivam D, Smith DF, Srinivasamoorthy G, Stoeckert CJ, Subramanian S, Thibodeau R, Tivey A, Treatman C, Velarde G, Wang H.** 2010. TriTrypDB: a functional genomic resource for the trypanosomatidae. Nucleic Acids Res **38**: D457–D462. http://dx.doi.org/10.1093/nar/gkp851.

49. **Ivens AC, Peacock CS, Worthey EA, Murphy L, Aggarwal G, Berriman M, Sisk E, Rajandream MA, Adlem E, Aert R, Anupama A, Apostolou Z, Attipoe P, Bason N, Bauser C, Beck A, Beverley SM, Bianchettin G, Borzym K, Bothe G, Bruschi CV, Collins M, Cadag E, Ciarloni L, Clayton C, Coulson RM, Cronin A, Cruz AK, Davies RM, De Gaudenzi J, Dobson DE, Fazelina G, Fosker N, Frasch AC, Fraser A, Fuchs M, Gabel C, Goble A, Goffeau A, Harris D, Hertz-Fowler C, Hilbert H, Horn D, Huang Y, Klages S, Knights A, Kube M, Larke N, Litvin L, et al.** 2005. The genome of the kinetoplastid parasite, *Leishmania major*. Science **309**:436–442. http://dx.doi.org/10.1126/science.1112680.

50. **El-Sayed NM, Myler PJ, Bartholomeu DC, Nilsson D, Aggarwal G, Tran AN, Ghedin E, Worthey EA, Delcher AL, Blandin G, Westenberger SJ, Caler E, Cerqueira GC, Branche C, Haas B, Anupama A, Arner E, Aslund L, Attipoe P, Bontempi E, Bringaud F, Burton P, Cadag E, Campbell DA, Carrington M, Crabtree J, Darban H, da Silveira JF, de Jong P, Edwards K, Englund PT, Fazelina G, Feldblyum T, Ferella M, Frasch AC, Gull K, Horn D, Hou L, Huang Y, Kindlund E, Klingbeil M, Kluge S, Koo H, Lacerda D, Levin MJ, Lorenzi H, Louie T, Machado CR, McCulloch R, et al.** 2005. The genome sequence of *Trypanosoma cruzi*, etiologic agent of Chagas disease. Science **309**:409–415. http://dx.doi.org/10.1126/science.1112631.

51. **Panigrahi AK, Ogata Y, Zíková A, Anupama A, Dalley RA, Acestor N, Myler PJ, Stuart KD.** 2009. A comprehensive analysis of *Trypanosoma brucei* mitochondrial proteome. Proteomics **9**:434–450. http://dx.doi.org/10.1002/pmic.200800477.

52. **Besteiro S, Barrett MP, Rivière L, Bringaud F.** 2005. Energy generation in insect stages of *Trypanosoma brucei*: metabolism in flux. Trends Parasitol **21**:185–191. http://dx.doi.org/10.1016/j.pt.2005.02.008.

53. **Liu B, Molina H, Kalume D, Pandey A, Griffith JD, Englund PT.** 2006. Role of p38 in replication of *Trypanosoma brucei* kinetoplast DNA. Mol Cell Biol **26**:5382–5393. http://dx.doi.org/10.1128/MCB.00369-06.

54. **Klingbeil MM, Motyka SA, Englund PT.** 2002. Multiple mitochondrial DNA polymerases in *Trypanosoma brucei*. Mol Cell **10**:175–186. http://dx.doi.org/10.1016/S1097-2765(02)00571-3.

55. **Chandler J, Vandoros AV, Mozeleski B, Klingbeil MM.** 2008. Stem-loop silencing reveals that a third mitochondrial DNA polymerase, POLID, is required for kinetoplast DNA replication in trypanosomes. Eukaryot Cell **7**:2141–2146. http://dx.doi.org/10.1128/EC.00199-08.

56. **Scocca JR, Shapiro TA.** 2008. A mitochondrial topoisomerase IA essential for late theta structure resolution in African trypanosomes. Mol Microbiol **67**:820–829. http://dx.doi.org/10.1111/j.1365-2958.2007.06087.x.

57. **Hines JC, Ray DS.** 2010. A mitochondrial DNA primase is essential for cell growth and kinetoplast DNA replication in *Trypanosoma brucei*. Mol Cell Biol **30**:1319–1328. http://dx.doi.org/10.1128/MCB.01231-09.

58. **Panigrahi AK, Zíková A, Dalley RA, Acestor N, Ogata Y, Anupama A,**

Myler PJ, Stuart KD. 2008. Mitochondrial complexes in *Trypanosoma brucei*: a novel complex and a unique oxidoreductase complex. Mol Cell Proteomics **7:**534–545. http://dx.doi.org/10.1074/mcp.M700430 -MCP200.

59. Concepción-Acevedo J, Luo J, Klingbeil MM. 2012. Dynamic localization of *Trypanosoma brucei* mitochondrial DNA polymerase ID. Eukaryot Cell **11:**844–855. http://dx.doi.org/10.1128/EC.05291-11.

60. Yurchenko V, Votýpka J, Tesařová M, Klepetková H, Kraeva N, Jirků M, Lukeš J. 2014. Ultrastructure and molecular phylogeny of four new species of monoxenous trypanosomatids from flies (Diptera: Brachycera) with redefinition of the genus *Wallaceina*. Folia Parasitol **61:**97–112. http://dx.doi.org/10.14411/fp.2014.023.

61. Gentle IE, Perry AJ, Alcock FH, Likić VA, Dolezal P, Ng ET, Purcell AW, McConnville M, Naderer T, Chanez AL, Charrière F, Aschinger C, Schneider A, Tokatlidis K, Lithgow T. 2007. Conserved motifs reveal details of ancestry and structure in the small TIM chaperones of the mitochondrial intermembrane space. Mol Biol Evol **24:**1149–1160. http://dx.doi.org/10.1093/molbev/msm031.

62. Singha UK, Hamilton V, Duncan MR, Weems E, Tripathi MK, Chaudhuri M. 2012. Protein translocase of mitochondrial inner membrane in *Trypanosoma brucei*. J Biol Chem **287:**14480–14493. http://dx.doi.org/10.1074/jbc.M111.322925.

63. Miyahira Y, Dvorak JA. 1994. Kinetoplastidae display naturally occurring ancillary DNA-containing structures. Mol Biochem Parasitol **65:**339–349. http://dx.doi.org/10.1016/0166-6851(94)90084-1.

64. Vondrušková E, van den Burg J, Zíková A, Ernst NL, Stuart K, Benne R, Lukeš J. 2005. RNA interference analyses suggest a transcript-specific regulatory role for mitochondrial RNA-binding proteins MRP1 and MRP2 in RNA editing and other RNA processing in *Trypanosoma brucei*. J Biol Chem **280:**2429–2438. http://dx.doi.org/10.1074/jbc.M405933200.

65. Smíd O, Horáková E, Vilímová V, Hrdy I, Cammack R, Horváth A, Lukeš J, Tachezy J. 2006. Knock-downs of iron-sulfur cluster assembly proteins IscS and IscU down-regulate the active mitochondrion of procyclic *Trypanosoma brucei*. J Biol Chem **281:**28679–28686. http://dx.doi.org/10.1074/jbc.M513781200.

66. Long S, Jirků M, Mach J, Ginger ML, Sutak R, Richardson D, Tachezy J, Lukeš J. 2008. Ancestral roles of eukaryotic frataxin: mitochondrial frataxin function and heterologous expression of hydrogenosomal *Trichomonas* homologues in trypanosomes. Mol Microbiol **69:**94–109. http://dx.doi.org/10.1111/j.1365-2958.2008.06260.x.

67. Paris Z, Changmai P, Rubio MA, Zíková A, Stuart KD, Alfonzo JD, Lukeš J. 2010. The Fe/S cluster assembly protein Isd11 is essential for tRNA thiolation in *Trypanosoma brucei*. J Biol Chem **285:**22394–22402. http://dx.doi.org/10.1074/jbc.M109.083774.

68. Siegel TN, Hekstra DR, Cross GA. 2008. Analysis of the *Trypanosoma brucei* cell cycle by quantitative DAPI imaging. Mol Biochem Parasitol **160:**171–174. http://dx.doi.org/10.1016/j.molbiopara.2008.04.004.

69. Englund PT. 1979. Free minicircles of kinetoplast DNA in *Crithidia fasciculata*. J Biol Chem **254:**4895–4900.

70. Ryan KA, Englund PT. 1989. Synthesis and processing of kinetoplast DNA minicircles in *Trypanosoma equiperdum*. Mol Cell Biol **9:**3212–3217.

71. Chowdhury AR, Zhao Z, Englund PT. 2008. Effect of hydroxyurea on procyclic *Trypanosoma brucei*: an unconventional mechanism for achieving synchronous growth. Eukaryot Cell **7:**425–428. http://dx.doi.org/10.1128/EC.00369-07.

72. Klein KG, Olson CL, Engman DM. 1995. Mitochondrial heat shock protein 70 is distributed throughout the mitochondrion in a dyskinetoplastic mutant of *Trypanosoma brucei*. Mol Biochem Parasitol **70:**207–209. http://dx.doi.org/10.1016/0166-6851(95)00013-Q.

73. Searle S, McCrossan MV, Smith DF. 1993. Expression of a mitochondrial stress protein in the protozoan parasite *Leishmania major*. J Cell Sci **104:**1091–1100.

74. Campos RM, Nascimento M, Ferraz JC, Pereira MM, Rocha PO, Thompson GM, Cysne-Finkelstein L, Figueiredo RC, de Melo Neto OP. 2008. Distinct mitochondrial HSP70 homologues conserved in various *Leishmania* species suggest novel biological functions. Mol Biochem Parasitol **160:**157–162. http://dx.doi.org/10.1016/j.molbiopara.2008.04.013.

75. Fisk JC, Li J, Wang H, Aletta JM, Qu J, Read LK. 2013. Proteomic analysis reveals diverse classes of arginine methylproteins in mitochondria of trypanosomes. Mol Cell Proteomics **12:**302–311. http://dx.doi.org/10.1074/mcp.M112.022533.

76. Wang J, Englund PT, Jensen RE. 2012. TbPIF8, a *Trypanosoma brucei* protein related to the yeast Pif1 helicase, is essential for cell viability and mitochondrial genome maintenance. Mol Microbiol **83:**471–485. http://dx.doi.org/10.1111/j.1365-2958.2011.07938.x.

77. Lai D-, Hashimi H, Lun Z-, Ayala FJ, Lukeš J. 2008. Adaptations of *Trypanosoma brucei* to gradual loss of kinetoplast DNA: *Trypanosoma equiperdum* and *Trypanosoma evansi* are petite mutants of *T. brucei*. Proc Natl Acad Sci U S A **105:**1999–2004. http://dx.doi.org/10.1073/pnas.0711799105.

78. Liu B, Wang J, Yaffe N, Lindsay ME, Zhao Z, Zick A, Shlomai J, Englund PT. 2009. Trypanosomes have six mitochondrial DNA helicases with one controlling kinetoplast maxicircle replication. Mol Cell **35:**490–501. http://dx.doi.org/10.1016/j.molcel.2009.07.004.

79. Sbicego S, Alfonzo JD, Estévez AM, Rubio MA, Kang X, Turck CW, Peris M, Simpson L. 2003. RBP38, a novel RNA-binding protein from trypanosomatid mitochondria, modulates RNA stability. Eukaryot Cell **2:**560–568. http://dx.doi.org/10.1128/EC.2.3.560-568.2003.

80. Hines JC, Ray DS. 2011. A second mitochondrial DNA primase is essential for cell growth and kinetoplast minicircle DNA replication in *Trypanosoma brucei*. Eukaryot Cell **10:**445–454. http://dx.doi.org/10.1128/EC.00308-10.

81. Downey N, Hines JC, Sinha KM, Ray DS. 2005. Mitochondrial DNA ligases of *Trypanosoma brucei*. Eukaryot Cell **4:**765–774. http://dx.doi.org/10.1128/EC.4.4.765-774.2005.

82. Liu B, Wang J, Yildirir G, Englund PT. 2009. TbPIF5 is a *Trypanosoma brucei* mitochondrial DNA helicase involved in processing of minicircle Okazaki fragments. PLoS Pathog **5:**e1000589. http://dx.doi.org/10.1371/journal.ppat.1000589.

83. Liu B, Yildirir G, Wang J, Tolun G, Griffith JD, Englund PT. 2010. TbPIF1, a *Trypanosoma brucei* mitochondrial DNA helicase, is essential for kinetoplast minicircle replication. J Biol Chem **285:**7056–7066. http://dx.doi.org/10.1074/jbc.M109.084038.

84. Saxowsky TT, Choudhary G, Klingbeil MM, Englund PT. 2003. *Trypanosoma brucei* has two distinct mitochondrial DNA polymerase beta enzymes. J Biol Chem **278:**49095–49101. http://dx.doi.org/10.1074/jbc.M308565200.

85. Rajão MA, Passos-Silva DG, DaRocha WD, Franco GR, Macedo AM, Pena SD, Teixeira SM, Machado CR. 2009. DNA polymerase kappa from *Trypanosoma cruzi* localizes to the mitochondria, bypasses 8-oxoguanine lesions and performs DNA synthesis in a recombination intermediate. Mol Microbiol **71:**185–197. http://dx.doi.org/10.1111/j.1365-2958.2008.06521.x.

86. Voos W. 2013. Chaperone-protease networks in mitochondrial protein homeostasis. Biochim Biophys Acta **1833:**388–399. http://dx.doi.org/10.1016/j.bbamcr.2012.06.005.

87. Wu Y, Brosh RM. 2012. DNA helicase and helicase-nuclease enzymes with a conserved iron-sulfur cluster. Nucleic Acids Res **40:**4247–4260. http://dx.doi.org/10.1093/nar/gks039.

88. Netz DJ, Stith CM, Stümpfig M, Köpf G, Vogel D, Genau HM, Stodola JL, Lill R, Burgers PM, Pierik AJ. 2012. Eukaryotic DNA polymerases require an iron-sulfur cluster for the formation of active complexes. Nat Chem Biol **8:**125–132. http://dx.doi.org/10.1038/nchembio.721.

89. Schimanski B, Nguyen TN, Günzl A. 2005. Highly efficient tandem affinity purification of trypanosome protein complexes based on a novel epitope combination. Eukaryot Cell **4:**1942–1950. http://dx.doi.org/10.1128/EC.4.11.1942-1950.2005.

90. Basu S, Netz DJ, Haindrich AC, Herlerth N, Lagny TJ, Pierik AJ, Lill R, Lukeš J. 2014. Cytosolic iron-sulphur protein assembly is functionally conserved and essential in procyclic and bloodstream *Trypanosoma brucei*. Mol Microbiol **93:**897–910. http://dx.doi.org/10.1111/mmi.12706.

91. Ntambi JM, Englund PT. 1985. A gap at a unique location in newly replicated kinetoplast DNA minicircles from *Trypanosoma equiperdum*. J Biol Chem **260:**5574–5579.